Monthly Notices
of the
ROYAL ASTRONOMICAL SOCIETY

MNRAS **429,** 1827–1839 (2013) doi:10.1093/mnras/sts470

The drivers of AGN activity in galaxy clusters: AGN fraction as a function of mass and environment

K. A. Pimbblet,[1,2]★ S. S. Shabala,[3] C. P. Haines,[4] A. Fraser-McKelvie[1,2] and D. J. E. Floyd[1,2]

[1]*School of Physics, Monash University, Clayton, Victoria 3800, Australia*
[2]*Monash Centre for Astrophysics (MoCA), Monash University, Clayton, Victoria 3800, Australia*
[3]*School of Mathematics & Physics, University of Tasmania, Private Bag 37, Hobart, Tasmania 7001, Australia*
[4]*Steward Observatory, University of Arizona, 933 North Cherry Avenue, Tucson, AZ 85721, USA*

Accepted 2012 November 21. Received 2012 November 20; in original form 2012 October 01

ABSTRACT

We present an analysis of optical spectroscopically identified active galactic nuclei (AGN) down to a cluster magnitude of $M^\star + 1$ in a sample of six self-similar Sloan Digital Sky Survey galaxy clusters at $z \sim 0.07$. These clusters are specifically selected to lack significant substructure at bright limits in their central regions so that we are largely able to eliminate the local action of merging clusters on the frequency of AGN. We demonstrate that the AGN fraction increases significantly from the cluster centre to $1.5R_{\rm virial}$, but tails off at larger radii. If only comparing the cluster core region to regions at $\sim 2R_{\rm virial}$, no significant variation would be found. We compute the AGN fraction by mass and show that massive galaxies (log(stellarmass) >10.7) are host to a systematically higher fraction of AGN than lower mass galaxies at all radii from the cluster centre. We attribute this deficit of AGN in the cluster centre to the changing mix of galaxy types with radius. We use the WHAN diagnostic to separate weak AGN from 'retired' galaxies in which the main ionization mechanism comes from old stellar populations. These retired AGN are found at all radii, while the mass effect is much more pronounced: we find that massive galaxies are more likely to be in the retired class. Further, we show that our AGN have no special position inside galaxy clusters – they are neither preferentially located in the infall regions nor situated at local maxima of galaxy density as measured with Σ_5. However, we find that the most powerful AGN (with [O III] equivalent widths <-10 Å) reside at significant velocity offsets in the cluster, and this brings our analysis into agreement with previous work on X-ray-selected AGN. Our results suggest that if interactions with other galaxies are responsible for triggering AGN activity, the time lag between trigger and AGN enhancement must be sufficiently long to obfuscate the encounter site and wipe out the local galaxy density signal.

Key words: galaxies: active – galaxies: clusters: general – galaxies: evolution.

1 INTRODUCTION

Active galactic nuclei (AGN) are typically found inside massive galaxies that exhibit significant, ongoing or recent, star formation (Kauffmann et al. 2003; Jahnke et al. 2004; Heckman et al. 2005; von der Linden et al. 2010; Floyd et al. 2012). The power source for AGN is expected to be gas accretion on to a massive black hole (Lynden-Bell 1969) which suggests that black hole and galaxy spheroidal growth are closely linked (cf. Richstone et al. 1998; Kauffmann et al. 2003).

Mergers have frequently been cited as a method to fuel AGN (e.g. Sanders et al. 1988) and a number of morphological studies claim an excess of post-merger systems in their AGN samples (Bahcall et al. 1997; Canalizo & Stockton 2001; Urrutia et al. 2008; Letawe et al. 2010; Smirnova et al. 2010). Given that the fuel source for AGN is in the gas phase, any physical mechanism that has the potential to disturb the morphology of a galaxy such as harassment (Moore et al. 1996) may also produce an enhancement of AGN activity – i.e. not simply mergers. Since such physical mechanisms can be tied to environment, AGN may therefore be thought of as signposts to galaxy evolution in some circumstances (cf. Reichard et al. 2009). Indeed, there is extensive literature supporting the idea that AGN (defined in various ways using different wavelengths) are influenced by environment. For instance, Kauffmann et al. (2004)

★ E-mail: Kevin.Pimbblet@monash.edu

report that the fraction of optical spectroscopic AGN is markedly different for galaxies in different density regimes (explicitly: the AGN fraction decreases as a function of increasing local galaxy density; see also Montero-Dorta et al. 2009). This is supported by a study of 51 galaxy clusters by Ruderman & Ebeling (2005) who find an excess of X-ray point sources within 3.5 Mpc of the centre of galaxy clusters in comparison to control samples which they attribute to AGN that have been triggered by close encounters with neighbouring galaxies. This broadly supports an increase of AGN fraction with increasing galaxy density, but they divide this excess into two regions: near the cluster core where galaxies are interacting with the brightest cluster member, and at around the virial radius whose excess they report is attributable to low-energy collisions at the cluster-field boundary. Further, Popesso & Biviano (2006) detail an anticorrelation between cluster AGN fraction and cluster velocity dispersion (see also Sivakoff et al. 2008). They contend that this anticorrelation indicates that the merger rate of clusters affects the AGN fraction since AGN are likely to have played a strong hand in heating the intracluster medium and thereby drive evolution in subgroups that eventually form clusters (cf. Mamon 1992). From an investigation of the Abell 901/902 system, Gilmour et al. (2007) show that there is a deficit of AGN in the highest density regions that supports the above works and other investigations of cluster AGN locations (see Gisler 1978; Dressler, Thompson & Shectman 1985; Coldwell, Martínez & Lambas 2002; Georgakakis et al. 2008; Gavazzi, Savorgnan & Fumagalli 2011; Pimbblet & Jensen 2012). Naively, such a trend makes sense since galaxies in cluster centres would be more stripped of cold gas that can fuel an AGN than on cluster outskirts (see also Constantin et al. 2008; Lietzen et al. 2011).

Equally, there is an increasing body of literature that indicates that the opposite is true: environment plays little or no role in the frequency of AGN. Examining X-ray emission from clusters, Miller et al. (2003) find no evidence for an enhanced cluster AGN fraction. This is supported by spectroscopic work on eight clusters by Martini, Mulchaey & Kelson (2007) who detail that the AGN fraction is no lower in cluster centres than a control field sample. Although some of this may be caused by mass selection effects (cf. Pasquali et al. 2009; Pimbblet & Jensen 2012), Haggard et al. (2010) demonstrate that there is no significant difference in AGN fraction between cluster and field samples for a constrained range of absolute magnitudes. This is supported by von der Linden et al. (2010) who examine >500 Sloan Digital Sky Survey (SDSS; Abazajian et al. 2009) clusters and find no trend in AGN fraction with distance from cluster centres (see also Atlee et al. 2011; Klesman & Sarajedini 2012).

In this work, we present a new analysis of the AGN fraction's dependence on environment and mass to elucidate the issues summarized above using a sample of low-redshift SDSS galaxy clusters that are free from known structure contamination. In Section 2 we detail the data set that we use in this investigation. In Section 3, we compute how the AGN fraction varies with radius from the cluster centre and galaxy mass before discussing and summarizing our results in Section 4. Throughout this work, we adopt a standard, flat cosmology with $\Omega_{\rm M} = 0.238$, $\Omega_{\Lambda} = 0.762$ and $H_0 = 73$ km s^{-1} Mpc^{-1} (Spergel et al. 2007).

2 DATA SET

Since mergers of galaxy clusters or subclusters may locally enhance AGN activity, we require a sample of clusters that are relatively free from such activity. In Pimbblet (2011), we presented a sample of 14 such SDSS galaxy clusters derived from the earlier work of Plionis, Tovmassian & Andernach (2009) that have no merging or significant interaction with other (comparable) structures within the limits of SDSS observations. In brief, Pliois et al. (2009) use the criteria and catalogue of Andernach et al. (2005) to generate a 'clean' sample of Abell et al. (1989) clusters. This consists of considering the velocity distribution of each cluster in turn and its flatness (Struble & Ftaclas 1994), and also removal of any cluster with >1 X-ray peak. We refer the reader to Plionis et al. (2009) for a full description of this process.

Table 1. The cluster sample used in this work.

Name	RA (J2000)	Dec. (J2000)	$\overline{cz}$ (km s^{-1})	σ_{cz} (km s^{-1})	$R_{\rm virial}$ (Mpc)	$N(<3R_{\rm virial})$
A1205	11 13 58.1	+02 29 56	22 506	938	1.88	110
A1424	11 57 26.4	+05 05 52	22 764	780	1.56	78
A1620	12 50 03.0	−01 33 45	25 275	1007	2.01	153
A1650	12 58 34.7	−01 43 15	25 176	864	1.73	117
A1767	13 36 31.6	+59 08 51	21 111	988	1.98	111
A2670	23 54 13.7	−10 25 09	22 836	976	1.95	132

Here, we restrict the Pimbblet (2011) sample to six galaxy clusters that are within a narrow redshift slice ($0.070 < z < 0.084$; Table 1). The reason for selecting such a narrow sample to work with is to create a composite stacked cluster whose variation in absolute magnitude that corresponds to a given apparent magnitude completeness limit is small – no more than $\Delta M_R = 0.4$ (Pimbblet 2011). In terms of look-back time, the difference between our highest and lowest redshift clusters is ∼0.1 Gyr.

In line with the SDSS spectroscopic limit (see Strauss et al. 2002; Abazajian et al. 2009), we use a limiting magnitude of $r = 17.77$ in this work. Fig. 1 demonstrates that at $r = 17.77$, SDSS spectroscopy is still >90 per cent complete for our cluster sample (cf. Strauss et al. 2002; Jensen & Pimbblet 2012; Pimbblet & Jensen 2012). Further, Pimbblet (2011) notes that the sample covers little more than a factor of 2 in cluster mass. Combined with the small difference in look-back time, this ensures that the clusters in our sample are reasonably self-similar and are broadly at a comparable evolutionary stage.

In Table 1, we give the global properties of the clusters used in this work, including mean recession velocity ($\overline{cz}$), cluster velocity dispersion (σ_{cz}) and virial radius ($R_{\rm virial}$). The former two are based on Miller et al. (2005) whilst the virial radius is computed from σ_{cz} using the relation presented by Girardi et al. (1998). Cluster membership is then simplistically defined to be all galaxies within $\pm 3\sigma_{cz}$ of $\overline{cz}$. The number of galaxies in each cluster within $< 3R_{\rm virial}$ is reported as $N(< 3R_{\rm virial})$ in Table 1. These numbers are approximately the same as those reported by Pimbblet et al. (2006; see their table 2) for rich, X-ray luminous clusters at $z \sim 0.1$.

To create our final sample, we stack all of our clusters together to form a composite sample. Analogous to Pimbblet (2011), this is achieved by placing the clusters on to a common scale (i.e. $R_{\rm virial}$) and limiting our clusters to a common absolute magnitude (i.e. the absolute magnitude corresponding to $r = 17.77 - M_r = -19.96$ – at the redshift of our most distant cluster, Abell 1620; this corresponds to approximately $M^* + 1$ along the luminosity function according to the analysis of Jensen & Pimbblet 2012). As the terminal step, we select a mass limit for our clusters to prevent our sample being biased from having a low *r*-band limit that is coupled with a top-end mass limit (Holden et al. 2007; see also Pimbblet & Jensen 2012). To achieve this, we examine plots of absolute magnitude versus stellar mass for each of our clusters and restrict our sample to those

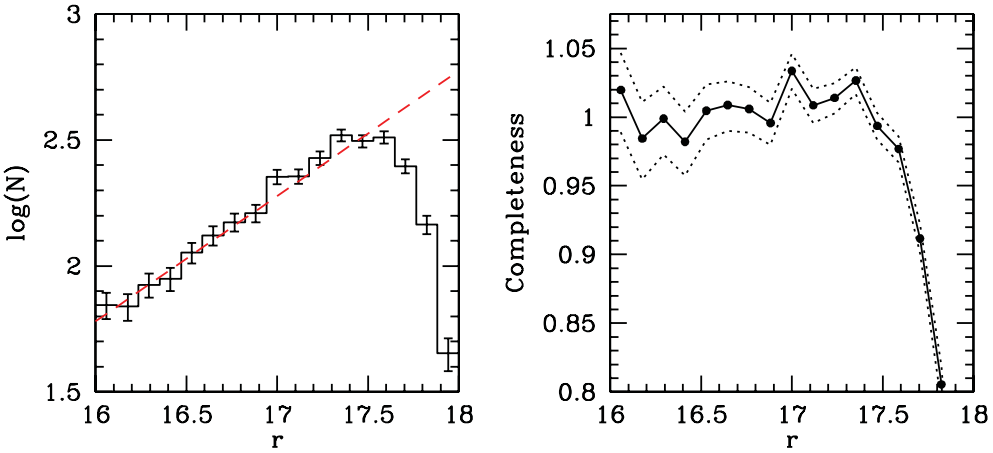

Figure 1. A histogram of *r*-band magnitudes (with Poisson errors) for our sample is displayed in the left-hand panel. A line of best fit (dashed line) is fitted to the linearly increasing region of this plot (i.e. $16.0 < r < 17.0$) which is used to create a completeness diagnostic plot (right-hand panel). The points in the right-hand panel denote the ratio of log (*N*) in the left-hand panel to line of best fit. The dotted lines enclosing these points denote the 1σ error of the completeness values. At our adopted limiting magnitude of $r = 17.77$, the spectroscopy is still >90 per cent complete.

galaxies brighter than $M_r = -19.96$ and more massive than the most massive galaxy log(stellarmass) = 10.4 at this limiting magnitude for our most distant cluster (Fig. 2).

The final, bias-corrected composite sample consists of 300 galaxies within $R_{\rm virial}$, and 701 galaxies within $3R_{\rm virial}$ from these 6 clusters.

2.1 Sample validation

Before proceeding with our analysis, we elect to perform some validation tests on our sample to ensure that they are free of substructure – at least in their centres – as we have suggested. The need for such a validation step is our concern that the literature expresses both ambiguous and conflicting statements about some of the clusters in our sample. For example, Abell 1650 is noted by Einasto et al. (2012) as being a unimodal cluster, in agreement with Pimbblet et al. (2002) who term it a morphologically regular cluster using a large radii data set. This is in contrast to Flin & Krywult (2006) who note that Abell 1650 has 'substructures in the cluster field'.

Taking our bias-corrected sample, we apply the Dressler & Shectman (1988, DS) test for substructure to each cluster individually. The DS test is probably the most powerful test available to detect substructure in arbitrary three-dimensional data sets (Pinkney et al. 1996) and we therefore consider it perfectly adequate for our sample validation check. Briefly, the DS test works by finding the local mean velocity and standard deviation of the 10 nearest neighbours to a given galaxy and compares them to the global values for the cluster, such that:

$$\delta^2 = \left(\frac{N_{\rm local}+1}{\sigma^2_{\rm global}}\right)[(\overline{cz}_{\rm local} - \overline{cz}_{\rm global})^2 + (\sigma_{\rm local} - \sigma_{\rm global})^2], \quad (1)$$

where the parameter δ yields a measure of the deviancy of this subsample. A summed parameter of merit, Δ, is then computed by summing all δ_i terms in each cluster. To get a handle on the probability of Δ occurring, the velocity data are shuffled randomly between member galaxies 1000 times in a Monte Carlo fashion and the actual value of Δ is then compared to this ensemble.

In Table 2, we give the values of $P(\Delta)$ for the clusters in our sample. All of our clusters are substructure free within $1R_{\rm virial}$ to the limits probed by our investigation. However, Abell 1620

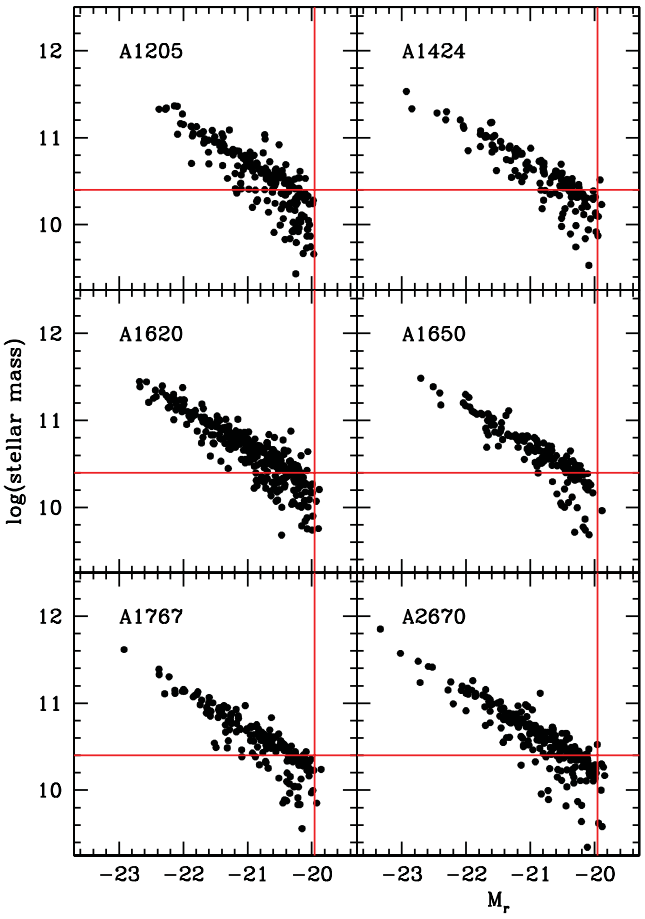

Figure 2. Absolute *r*-band magnitude versus galaxy stellar mass (expressed as the logarithm of the solar mass of the galaxy) for the clusters in our sample. The vertical line denotes the spectroscopic limit of $r = 17.77$ in our most distant cluster (Abell 1620) and the horizontal line denotes log(stellarmass) = 10.4 that corresponds to the mass limit that we are ∼ complete to. These lines are replicated for the other five clusters. We only use galaxies that are more massive and brighter than these limits for our subsequent analysis to avoid biasing our sample.

Table 2. Results of the DS test using various cuts in radii. Results under 0.01 are considered to indicate significant substructure.

Cluster	$P(\Delta)$		
	$r < R_{\rm virial}$	$r < 2R_{\rm virial}$	$r < 3R_{\rm virial}$
A1205	0.39	0.12	0.08
A1424	0.20	0.03	0.05
A1620	0.03	<0.01	<0.01
A1650	0.05	0.05	0.21
A1767	0.38	0.34	0.33
A2670	0.25	0.31	0.29

stands out from the others as possessing significant substructure at high radii from the cluster centre. This agrees with the analysis of Burgett et al. (2004) who also suggested that the cluster may contain substructure from a complementary analysis of 2 degree field data. We analyse this cluster further in Appendix A. Despite the substructure at high cluster-centric radii, we retain Abell 1620 in our sample. We have experimented with removing this cluster from our sample and find that the effect on our primary results is negligible, but our uncertainties become fractionally larger.

Finally, we issue the caveat that even though this simplistic test has indicated no substructure in the centres of our clusters, this does not preclude substructure at fainter magnitude limits arising from coherent, potentially low-mass, infalling groups as might be expected (cf. Owers et al. 2011).

2.2 AGN identification

In order to identify which galaxies in our sample are AGN, we make use of a BPT diagram (Baldwin, Phillips & Terlevich 1981; see also Veilleux & Osterbrock 1987). The BPT plane consists of flux ratio of $[\mathrm{N\ II}]_{\lambda6583}/\mathrm{H}\alpha$ versus $[\mathrm{O\ III}]_{\lambda5007}/\mathrm{H}\beta$. The measurements of equivalent widths for these lines are taken from Tremonti et al. (2004, see also www.mpa-garching.mpg.de/SDSS). In Fig. 3 we plot the position of all galaxies in the composite cluster on the BPT plane that have S/N > 3 in the necessary lines. To differentiate AGN from galaxies that are simply star forming, we use the demarcation curve of Kauffmann et al. (2003). The curve is a refinement of earlier work by Kewley et al. (2001) and yields 30 AGN within $R_{\rm virial}$ and 81 AGN within $3R_{\rm virial}$. We also define a composite sample – those galaxies that lie between the Kaufmann and Kewley curves – these galaxies are weaker AGN whose host galaxies are star forming. By implication, the use of the BPT diagram to select AGN means that our sample are composed of 'cold-mode' AGN (cf. Kereš et al. 2005; Hopkins & Hernquist 2006).

From the outset, we note that there is no significant optical colour difference (e.g. in $g - r$) between our AGN sample and the rest of the cluster population. This holds true even if we divide our sample by galaxy stellar mass.

3 AGN FRACTION

We now compute the cluster AGN fraction in two ways: by radius from the centre of the cluster and by galaxy mass. We note that the stellar masses of the galaxies are from the SDSS value-added catalogue (www.mpa-garching.mpg.de/SDSS; see also Kauffmann et al. 2003).

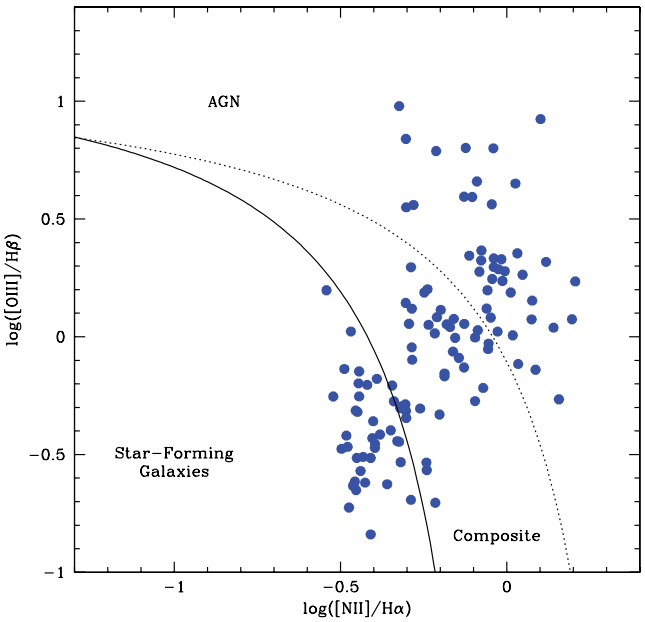

Figure 3. BPT plane for our composite cluster galaxy sample. All points have S/N >3 in each line. The solid curve is the Kauffmann et al. (2003) demarcation line: galaxies above the curve are designated AGN, those below are simply regular star-forming galaxies. Also shown is the Kewley et al. (2001) demarcation curve (dotted line). Galaxies between the two curves are composites: weaker AGN whose hosts are also star forming.

3.1 Fraction by radius from cluster centre

From the outset of our analysis, we note that we have selected the brightest cluster member as being the centre of our galaxy clusters. Although other choices could have been made, such as a luminosity-weighted centre or the peak X-ray flux location, we note that varying this choice does not alter the primary results presented in this work. We compute the AGN radial fraction in terms of $R_{\rm virial}$ (a more physically meaningful scale than a fixed metric that uses Mpc; cf. Pimbblet et al. 2002) and plot the result in Fig. 4. The AGN fraction is found to increase with distance from the cluster centre at a rate of $\mathrm{d(fraction)}/\mathrm{d}R_{\rm virial} = 0.018 \pm 0.020$.

This rate of increase is not significant, which may explain some of the differences reported in the literature concerning this fraction [for instance, contrast Gilmour et al. (2007) and Kauffmann et al. (2004) with Miller et al. (2003) and Martini et al. (2007). That said, if we restricted our analysis to the three innermost points of Fig. 4 (i.e. $<1.5R_{\rm virial}$), we find a significant gradient of $\mathrm{d(fraction)}/\mathrm{d}R_{\rm virial} = 0.064 \pm 0.021$. For those studies that split the radial AGN fraction into bins similar to our analysis (Coldwell et al. 2002), similar results are obtained.

Further, if we were to compare the AGN fraction within $1.5R_{\rm virial}$ to that at 2.0–$3.0R_{\rm virial}$, we find no significant difference (AGN fractions of 0.11 ± 0.02 and 0.11 ± 0.03, respectively). This may explain why investigations that compare the 'cluster' environment to a control 'field' may be biased to finding no difference in AGN fraction. Moreover, the types of clusters used can also bias the measurement of AGN fraction – those investigations that use all types of clusters to probe that AGN fraction could be biased by the presence of substructure – a bias that the present work intentionally avoids – as could the use of very high central density clusters versus low density.

The lines of best fit presented in Fig. 4 could also be oversimplifications of the situation. For example, Porter et al. (2008) report

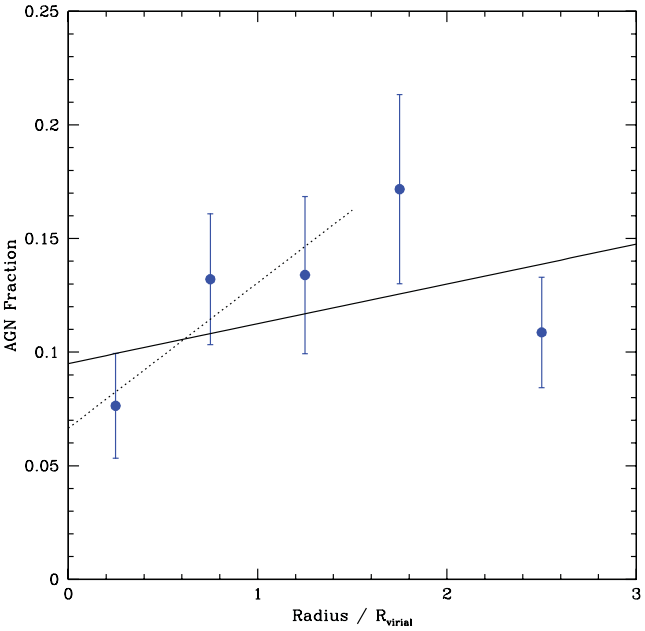

Figure 4. AGN fraction in the composite cluster as a function of radius from the centre, with Poisson errors. Each bin covers $0.5R_{\rm virial}$ except the last bin that covers $1R_{\rm virial}$ to ensure that each point in the plot has >100 member galaxies (cf. Cameron 2011). A line of best fit to these points is overplotted as the solid line. This line has a gradient of $\mathrm{d(fraction)}/\mathrm{d}R_{\rm virial} = 0.018 \pm 0.020$. We also display a line of best fit to the three points within $1.5R_{\rm virial}$ (dotted line), which has a gradient of $\mathrm{d(fraction)}/\mathrm{d}R_{\rm virial} = 0.064 \pm 0.021$.

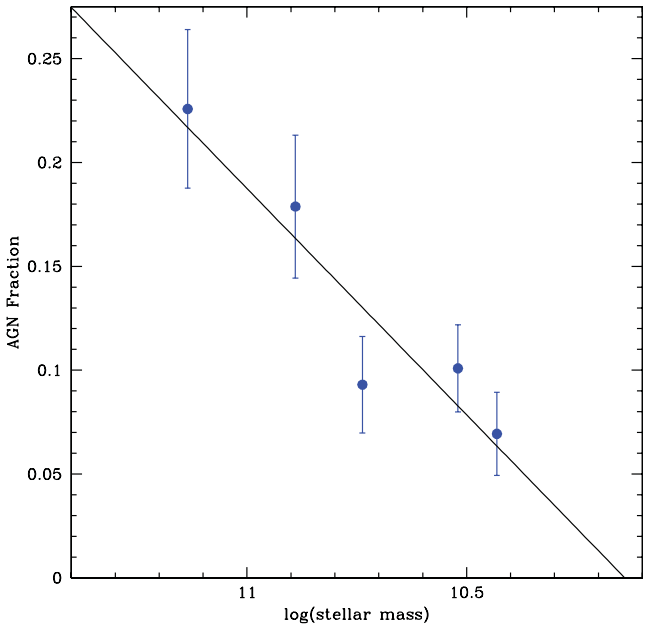

Figure 5. Same as Fig. 4, but as a function of galaxy stellar mass; each point has the same number of galaxies. The line of best fit has a gradient of $\mathrm{d(fraction)}/\mathrm{d}\log(\mathrm{stellarmass}) = 0.22 \pm 0.05$ across the range studied.

that there is an enhancement of specific star formation rate (SFR) at ∼few Mpc away from cluster centres caused by harassment inside galaxies being accreted along filaments of galaxies (see also Koyama et al. 2008; Perez et al. 2009). If true, then we may expect a similar enhancement of AGN fraction just beyond the virial radii of our clusters. Although Fig. 4 displays a local maxima in AGN fraction at $1.75R_{\rm virial}$, it is not significant – a larger sample of clusters and bona fide filaments will be required to fully address this question.

3.2 Fraction by mass

In Fig. 5 we compute the AGN fraction as a function of galaxy stellar mass for all galaxies within $3R_{\rm virial}$. We fit these data with a line of best fit and find that it has a significant gradient of $\mathrm{d(fraction)}/\mathrm{d}\log(\mathrm{stellarmass}) = 0.22 \pm 0.05$ – higher mass galaxies are significantly more likely to host AGN than their lower mass cousins (cf. Dunlop et al. 2003; Floyd et al. 2004; Brusa et al. 2009; Xue et al. 2010; Pimbblet & Jensen 2012; Tanaka 2012; see also Best et al. 2005).

To examine if a mass selection would affect the radial cluster AGN fraction, we repeat our above radial analysis for two mass bins in Fig. 6, split (arbitrarily) at $\log(\mathrm{stellarmass}) = 10.7$, to ensure that there are approximately equal numbers of galaxies above and below that mass in our sample. The more massive galaxies have a larger AGN fraction at all radii and there is a steady (but not very significant) increase in AGN from the cluster centre to $2R_{\rm virial}$ before it drops slightly lower again. Conversely, the lower mass galaxies do not vary in fraction significantly. The deficit of AGN in the centre of clusters may therefore simply be a reflection of the changing mix of galaxy types (e.g. colour, morphology, mass) with cluster radius (cf. von der Linden et al. 2010). This is illustrated in Table 3, where

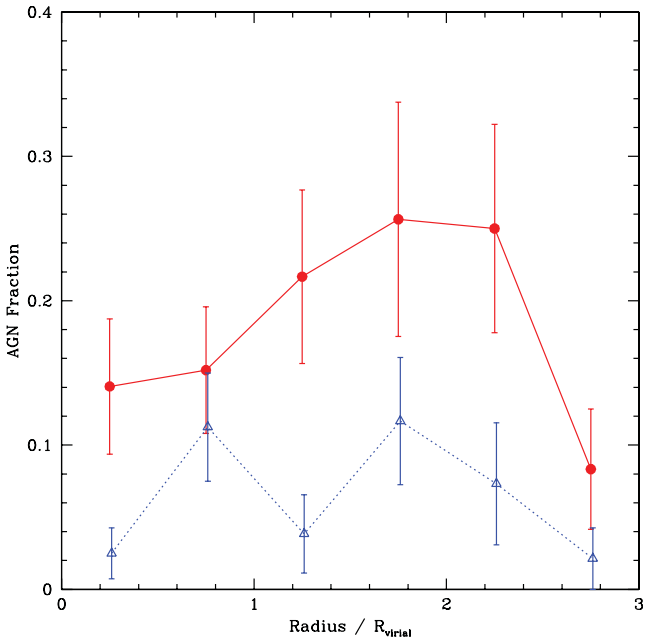

Figure 6. Same as Fig. 4, but for galaxies with log(stellar mass) >10.7 (filled red circles, solid line) and <10.7 (open blue triangles, dotted line). The higher mass regime contains a higher fraction of AGN at all radii.

we note that the fraction of galaxies with log(stellarmass) >11.0 in our sample steadily decreases with radius from the centre of our stacked cluster. This covariance of radius with mass is simply an expression of the well-known morphology–density relation (e.g., Dressler 1980; Dressler et al. 1997; Smith et al. 2005; see also Baldry et al. 2006).

Table 3. Illustration of how the fraction of our most massive galaxies (log(stellar mass) >11.0) in our sample changes as a function of radius.

Radius ($R_{\rm virial}$)	Fraction
0–1	0.19 ± 0.02
1–2	0.16 ± 0.03
2–3	0.14 ± 0.03

4 DISCUSSION

4.1 AGN phase space and local galaxy density

If AGN fractions are being enhanced in the cluster outskirts by interactions with other galaxies, then an investigation of their locations in $(cz - \overline{cz})/\sigma_{cz}$ versus radius/$R_{\rm virial}$ phase space may reveal this. This phase space is plotted in Fig. 7. We test if the AGN and other galaxy populations are distributed differently on this plane through a two-dimensional Kolmogorov–Smirnov (K-S) test (Peacock 1983; Fasano & Franceschini 1987) and find that the two populations are the same – i.e. the AGN are no more likely to be at large values of $|(cz - \overline{cz})|/\sigma_{cz}$ plus radius/$R_{\rm virial}$ (or conversely, centrally concentrated) than other cluster galaxies. This holds even if we consider only galaxies more massive (or less massive) than log(stellarmass) = 10.7. Indeed, both the mean and median values of $|(cz - \overline{cz})|/\sigma_{cz}$ for the AGN and general cluster population are within 1σ of each other, even within individual $1R_{\rm virial}$ radial bins.

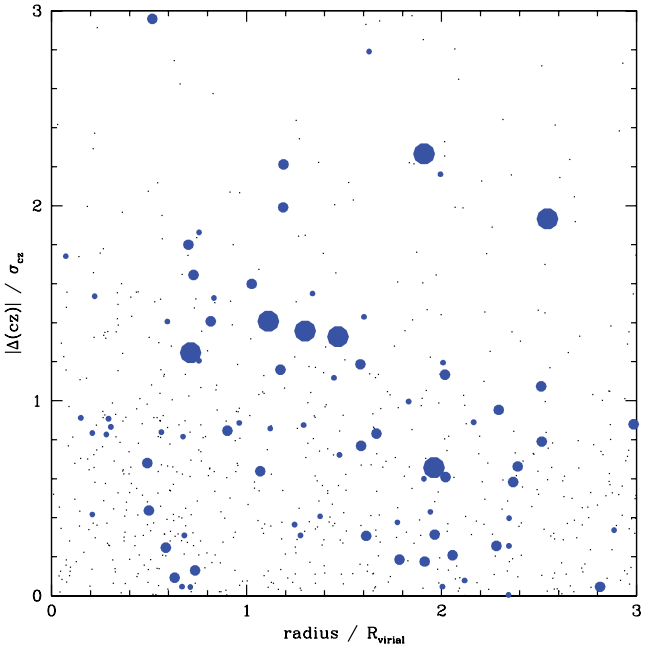

Figure 7. Phase-space diagram of AGN and other cluster members (dots) on a $\Delta(cz)$ versus radius plane. The AGN are coded according to their [O III] emission. The largest blue points are AGN with an equivalent width of [O III] <-10 Å; the medium-sized points have [O III] equivalent widths in the range from -1.5 to -10 Å; all the other (smallest) blue points have [O III] equivalent width >-1.5 Å.

These results are in apparent disagreement with Haines et al. (2012; see especially their fig. 6) who find that X-ray-selected AGN are significantly more likely to be at the cluster infall regions than the general cluster population. Apart from using X-ray-selected AGN, Haines et al. (2012) also use different cluster selection criteria: their clusters are more massive than the ones employed here and at higher redshift – the mean difference in look-back time between our sample and Haines et al. is $\approx$1.7 Gyr – and the clusters may possess significant subclustering even at bright magnitudes. On the other hand, finding several AGN at comparatively low velocity offsets and radii is not absolute proof against them being an infalling population, as they can easily still appear at these locations (see fig. 10 of Haines et al. 2012). An alternative hypothesis is that the AGN at low radii and velocity offsets are 'retired galaxies' – i.e. galaxies whose ionization mechanism is provided by old stellar populations (e.g. Cid Fernandes et al. 2010, 2011; Yan & Blanton 2012 and references therein). In Fig. 8 we plot our sample using the WHAN diagnostic plot of Cid Fernandes et al. (2011). This plot is more 'efficient' than the standard BPT approach as it only uses two lines: Hα and [N II]. Moreover, it is readily able to disentangle the so-called retired galaxy population from weak AGN types. The WHAN diagram can also classify up to 50 per cent more of the emission line galaxy types than the BPT approach, and is therefore more able to distinguish LINERs from Seyferts, but no information from the BPT is 'lost' in the move to the WHAN diagnostic.

There are a number of noteworthy aspects of Fig. 8. At a basic level, it reflects already well-known results that actively star-forming galaxies reside at the outskirts of clusters (i.e. there are fractionally fewer circled dots in the star-forming corner compared the passive population), whereas the passive galaxies dominate the low velocity offset, low radii population (cf. Pimbblet et al. 2006; Pimbblet & Jensen 2012 and references therein). Of our AGN population, some 35 ± 6 per cent fall into the 'retired' classification. These AGN are not preferentially situated at low radii and low velocity offsets: only 36 ± 10 per cent of the retired AGN satisfy such a criterion. This is, however, a slightly larger fraction than the other AGN classes: 14 ± 10 per cent of weak AGN and 16 ± 6 per cent of strong AGN reside at low radii plus low velocity offsets. These statistics are not significant enough to infer a duty cycle, but it is clear that all classes of AGN reside at all positions in our clusters.

We interrogate Fig. 8 to determine how the retired fraction of both AGN and the entire galaxy population varies as a function of radius from the cluster centre and galaxy mass and present these results in Table 4. Whilst the retired fraction of all galaxies is approximately constant with radius, the retired fraction of AGN mildly decreases with distance away from the centre of our clusters. The trend with mass is steeper: high-mass galaxies are much more likely to be in the retired class than lower masses. This result agrees with the contention of Lee et al. (2012) that the presence of a bar in a galaxy is no trigger for AGN activity (see also Combes 2003). Rather, the presence of bars and AGN is simply driven by host galaxy mass (e.g., Sheth et al. 2008; Nair & Abraham 2010).

Taking Figs 7 and 8 together, there is some suggestion that the disagreement with Haines et al. (2012) outlined above may not be so serious. By considering only those AGN with equivalent widths of [O III] <-10 Å, we see that they seem to lie above $|\Delta(cz)|/\sigma_{cz} = 1.2$ (Fig. 7). This is reflected in Fig. 8: those AGN with the highest Hα emission values have larger velocity offsets (i.e. those points that are not circled in Fig. 8). This holds in all three panels of Fig. 8 – i.e. at all radii. Haines et al. (2012) note that their (powerful, X-ray) AGN reside on infalling caustic; hence, if we only examine those powerful AGN in our sample, we come to an analogous conclusion.

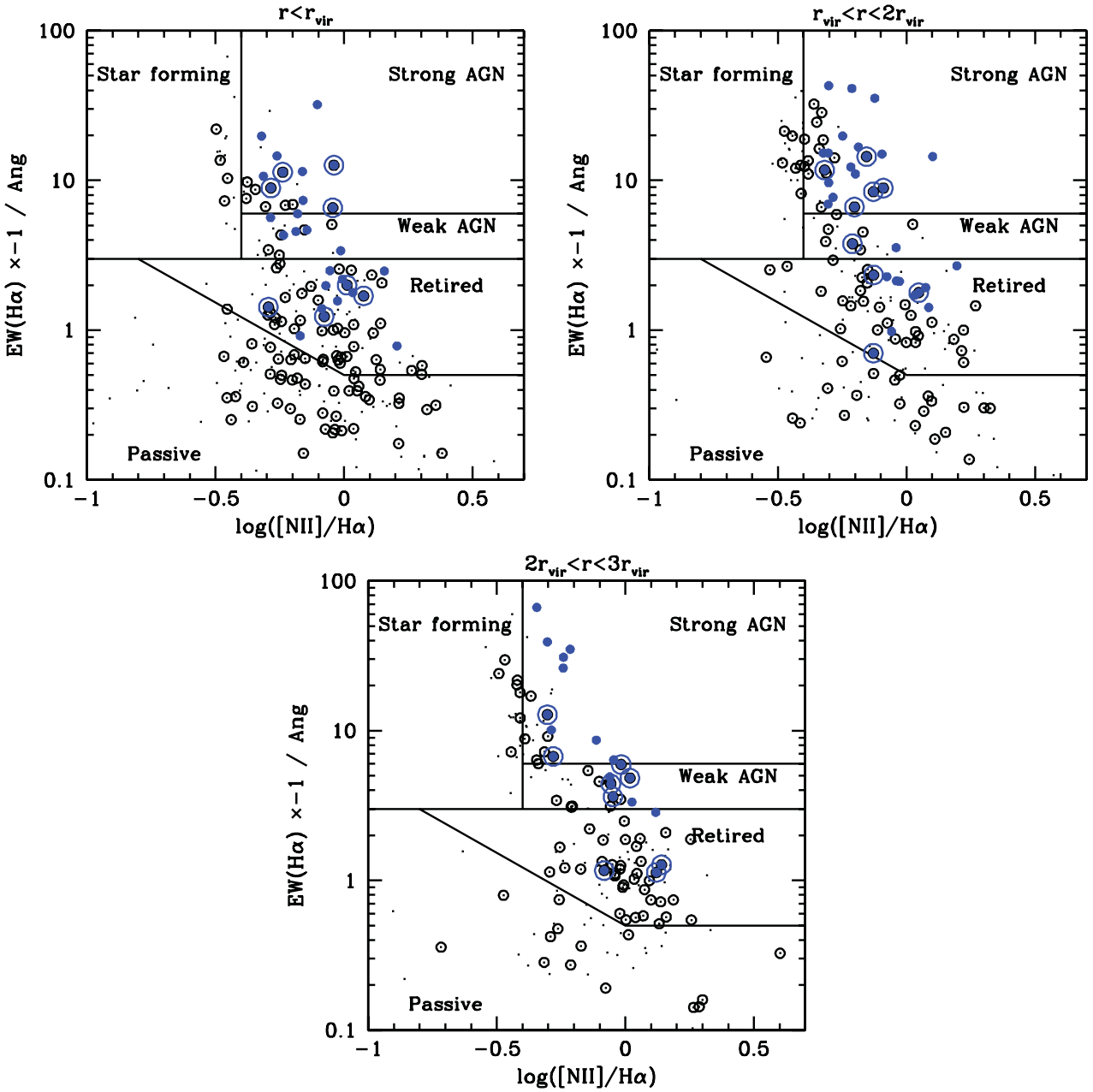

Figure 8. Diagnostic plot of Cid Fernandes et al. (2011) applied to our sample and split by radius. The larger blue points represent our AGN, as defined by the Kauffmann demarcation line. The small dots denote all our other galaxies, regardless of whether they have a high S/N ratio (i.e. unlike the definition of our AGN sample). The circled points denote low-velocity-offset galaxies with $|\Delta(cz)|/\sigma_{cz} < 0.5$. Although ∼35 per cent of our AGN may be retired galaxies under this classification, those AGN with low radii and velocity offset are not preferentially retired.

Table 4. Fraction of retired AGN and galaxies from the total population taken from Fig. 8 as a function of radius and galaxy mass. The mass bins are chosen to have approximately equal galaxy numbers in the total population.

Bin	Retired AGN fraction	Retired fraction of total population
0–1 $R_{\rm virial}$	0.45 ± 0.12	0.37 ± 0.04
1–2 $R_{\rm virial}$	0.34 ± 0.10	0.36 ± 0.04
2–3 $R_{\rm virial}$	0.20 ± 0.10	0.41 ± 0.05
log(stellar mass) > 10.809	0.51 ± 0.10	0.53 ± 0.05
10.575 < log(stellar mass) < 10.809	0.12 ± 0.08	0.34 ± 0.04
log(stellar mass) < 10.575	0.12 ± 0.08	0.26 ± 0.03

We can also examine if the AGN are preferentially in areas of high galaxy density by computing the local galaxy density for each galaxy in our sample. We choose Σ_5 – the surface area on the sky that is occupied by a given galaxy to its tenth nearest neighbour – as our estimator of local galaxy density; this is effectively a probe of the internal densities of the dark matter haloes (Muldrew et al. 2012). The plot of Σ_5 as a function of radius from the cluster centre is shown in Fig. 9. There are a number of obvious AGN at high local galaxy density, but to test whether the AGN are at a systematically higher value of Σ_5 we compare bootstrapped mean Σ_5 values of the AGN against the rest of the cluster members as a function of radius (Table 5). This shows no significant difference between the two populations at any radii.

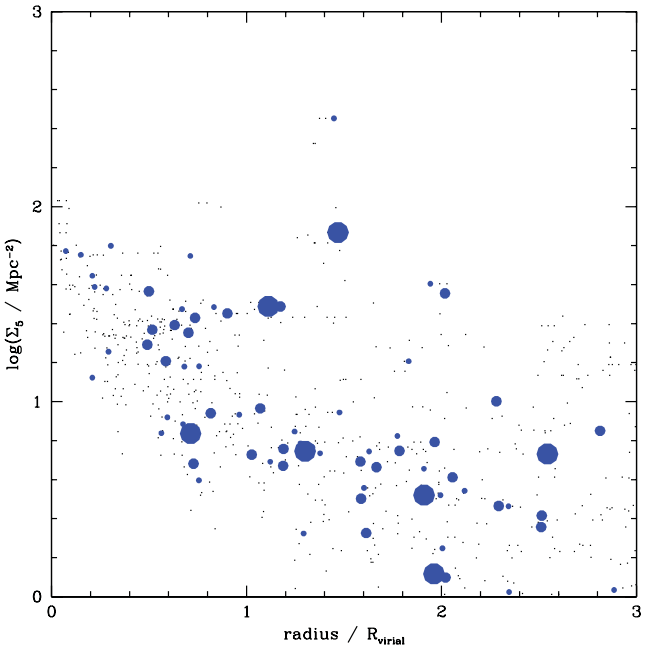

Figure 9. Local galaxy density, Σ_5, as a function of radius from the cluster centre. The large blue points denote the AGN, coded as per Fig. 7; the small dots show the other galaxies. The AGN statistically occupy the same region of this parameter space as the other cluster members (Table 5).

Table 5. Bootstrapped means and standard deviations of Σ_5 values for the AGN and other cluster members as a function of radius from the cluster centre. The two samples are statistically drawn from the same parent population.

Radius ($R_{\rm virial}$)	AGN Σ_5 (Mpc^{-2})	Other Σ_5 (Mpc^{-2})
0–0.5	56.4 ± 13.9	39.1 ± 5.6
0.5–1.0	18.4 ± 2.7	19.2 ± 1.5
1.0–1.5	35.2 ± 20.8	26.1 ± 5.3
1.5–2.0	4.3 ± 0.9	5.4 ± 0.6
2.0–2.5	8.8 ± 3.2	10.8 ± 2.2
2.5–3.0	3.0 ± 1.5	4.1 ± 1.7

Therefore, if AGN are being triggered by encounters with other galaxies, they have since moved away from the site of the interaction suggesting a suitably long time-scale between interaction and subsequent AGN enhancement. Detailed computation of the value of this time lag is beyond the scope of the present work, but we would expect it to be less than the time required for substructure to homogenize (e.g., Araya-Melo et al. 2009). Other studies (e.g. Schawinski et al. 2007; Shabala et al. 2012) have found that when interactions trigger AGN, it takes ∼100–200 Myr for an AGN to 'switch on'. Given a velocity dispersion of ∼1000 km s^{-1} (cf. Table 1), each galaxy could move 100–200 kpc in this time. Therefore, we regard it as comparatively easy to 'wipe out' the local density enhancement signature by the time the AGN switches on.

To round off this part of our discussion, we now cross-match our sample with the Faint Images of the Radio Sky at Twenty-Centimetres (FIRST) radio data base to ascertain which of our galaxies would be classified as radio AGN (or 'hot-mode') and determine their radial fractions. We find 28 matches from FIRST using a cross-matching radius of 10 arcsec to our sample. To see whether the detected radio emission can arise due to just star formation, we examine the SFR values for these galaxies from the value-added SDSS catalogues. We convert the reported SFR to a 1.4 GHz radio luminosity using the formula of Yun et al. (2001) and determine how much higher the FIRST radio luminosity was than the value expected purely from star formation. Radio AGN are then extracted as those galaxies whose FIRST radio luminosity exceeds that expected from the star formation within the SDSS fibre by a factor of $>1\sigma$ (where σ is the standard deviation in the SFR estimate). This results in 15 radio AGN. This sample has a markedly high mass: the median is $\log(\text{stellarmass}/\text{M}_\odot) = 11.2 \pm 0.3$. The radio AGN fraction for these galaxies goes as 0.013 ± 0.007, 0.028 ± 0.011 and 0.027 ± 0.012 for bins of $1R_{\rm virial}$ from the cluster centre. These small-number statistics are hard to draw a meaningful conclusion from.

4.2 Composite AGN and AGN power

In Fig. 3, we identified not only the AGN (those galaxies above the Kaufmann demarcation line), but also a sample of composite weak AGN and star-forming galaxies (those between the Kaufmann and Kewley demarcation lines). In Fig. 10 we divide the radial AGN fraction into the Kewley demarcated AGN and the composite sample to ascertain if the composite sample is driving any of the trends seen above. The composite sample appears to follow quite a flat distribution. Meanwhile, the Kewley et al. (2001) defined AGN show a steeper initial variation with increasing radius which plateaus quickly. Both samples are consistent with the trend depicted in Fig. 4 for the AGN fraction gradient. However, if we consider only the inner points (i.e. the dotted line in Fig. 4), we see that this is more consistent with the Kewley defined AGN.

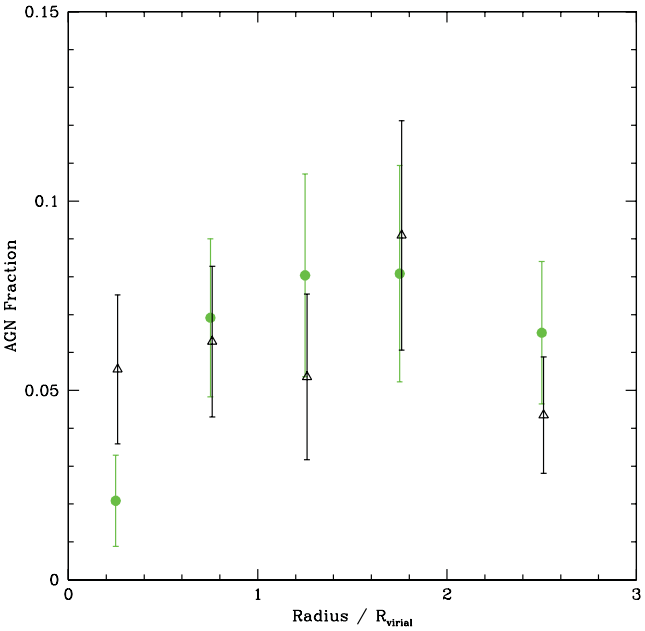

Figure 10. Same as Fig. 4, but split on the basis of whether the galaxies fall in the 'composite' AGN+star-forming sample (black open triangles) or the Kewley et al. (2001) definition of AGN (green filled circles). The two samples are fractionally offset in radius from each other for clarity.

Table 6. Variation of [O III] equivalent width (EW) with radius. The quoted uncertainties are bootstrapped standard deviations.

Radius ($R_{\rm virial}$)	AGN sample median [O III] EW (Å)	All galaxies median [O III] EW (Å)
0–1	-1.3 ± 0.2	-0.4 ± 0.1
1–2	-1.6 ± 0.7	-0.5 ± 0.1
2–3	-1.6 ± 0.7	-0.6 ± 0.1

If there is a bona fide radial trend of AGN fraction with radius, we may be able to see this reflected in the [O III] line strength which is a proxy for AGN power. In Table 6, we list the median equivalent widths of [O III] for our original AGN (i.e. Kauffmann delineated) with radius (see also the different point sizes in Figs 7 and 9). For comparison, we also detail the same measurement for all galaxies in our sample. No significant radial trend is observed for either sample. In the case of the AGN, this may simply be because we lack the numbers to detect such a trend since we only have 84 AGN within $3R_{\rm virial}$ (and a maximum of 32 galaxies in a 1 Mpc bin in Table 6). A larger sample will be required to investigate this. We can, however, infer that we are not missing any AGN because they are simply too weak and therefore below the BPT detection threshold. Hence, the change in AGN fraction is a bona fide change in the duty cycle rather than AGN luminosity.

4.3 AGN colour

If AGN are preferentially associated with bright galaxies that are presumably morphologically late type, then determining the fraction of AGN in radial bins in our sample should mimic the radial distribution of late-type galaxies in clusters – i.e. the morphology–density relation (Dressler 1980; see above) and therefore not address whether a specific mechanism is tied to AGN activation or quenching. To partially resolve this, we could attempt to morphologically classify all of our sample through using (e.g.) Galaxy Zoo (Lintott et al. 2008) in an analogous way to Pimbblet & Jensen (2012). But this approach contains problems: principal among them being a large fraction of 'uncertain' classifications that could skew an analysis. To combat this, we construct a colour–mass diagram for our sample, divided by radius to the cluster centre (Fig. 11). We divide this diagram up into two halves: a red sequence and a blue cloud component. This is done by eye, choosing a line that divides the two reasonably cleanly. Despite the arbitrary nature of this approach, it serves our purpose of creating two categories of galaxies (i.e. early and late types) and we note that the gradient is consistent with the colour–magnitude relations presented in earlier works (Pimbblet et al. 2002, 2006) and the lower envelope limit of such fitted colour–magnitude relations. However, we caution that we have made no attempt to correct the $(g - r)$ colours in Fig. 11 for AGN blueing: given the use of SDSS model magnitudes, we suggest that this effect would be small and only likely to affect the strong (i.e. bluest) AGN population since the weak and retired AGN are already predominantly residing on the red sequence (Fig. 11).

From Fig. 11, we see that any enhancement of the red sequence AGN fraction at low radii appears to be purely driven by massive galaxies. We quantify this in Table 7 where we detail the AGN fractions not only above and below the red sequence envelope cutoff, but also divided by mass. Although the uncertainties on these numbers are large (too large to infer statistically significant trends), by considering galaxies lying within and outside $1R_{\rm virial}$ of the cluster centre, it is tempting to speculate that red massive AGN and blue low-mass AGN may have a radial dependence whereas the red sequence low-mass AGN may not. If so, this may imply a common AGN triggering mechanism such as a gas-rich interaction. Hence, if a low-mass galaxy underwent such an interaction, it would necessarily become blue due to the parallel star formation. This would not be the case for a massive galaxy since it will have a lower specific SFR which in turn would correlate with the $(g - r)$ colour. A larger sample of clusters is required to unambiguously address this issue.

Finally, we note that disregarding the division by mass, at all radii, the fraction of AGN in the blue category is twice that in the red. This is broadly consistent with our earlier results that galaxies which show signatures of recent interactions show elevated levels of both AGN activity and blue colours (Kaviraj et al. 2012; Shabala et al. 2012).

5 SUMMARY

In summary, we have investigated the AGN fraction in six 'clean' galaxy clusters down to $\approx M^{\star} + 1$ as a function of both mass and radius from the cluster centre. Our main results are the following.

(i) The radial AGN fraction increases steeply in the central $1.5R_{\rm virial}$ of the composite cluster, but flattens off quickly and even decreases beyond this radius. If one were to compare the central regions of clusters with field samples, then no difference would be found on the basis of this work.

(ii) The AGN fraction by mass shows a significant trend such that more massive galaxies are more likely to host AGN. Indeed, massive galaxies host more AGN at all radii from the cluster centre. The reported deficit of AGN in cluster centres may therefore simply be a product of the changing mix of galaxy types with radius.

(iii) Retired AGN (found using the WHAN diagnostic) are found at all radii in the cluster, but their response to mass is much more pronounced: we find that massive galaxies are more likely to be in the retired class.

(iv) AGN have no preferential position inside galaxy clusters (either with regard to infalling status or enhanced local galaxy density). This conclusion can be brought into line with studies of X-ray AGN (e.g. Haines et al. 2012) by considering only the most powerful optical AGN. These galaxies avoid $|\Delta(cz)|/\sigma_{cz} < 1.2$ and may therefore reside on the cluster caustics (infall regions) as demonstrated in Haines et al. (2012).

(v) If interactions with other galaxies trigger AGN activity, then the time lag between the trigger and AGN enhancement must be sufficiently long to mask the site of the encounter and eliminate any signal in local galaxy density.

Our favoured scenario for AGN triggering remains a gas-rich interaction, although increased numbers of galaxies are required to produce better statistics to firm this speculation up.

ACKNOWLEDGMENTS

We thank the anonymous referee for his/her interesting feedback that improved this manuscript. We further thank David Atlee, Heath Jones and Duncan Galloway for stimulating conversations on this work.

SSS thanks the Australian Research Council for the award of a Super Science Fellowship at the University of Tasmania. DJEF

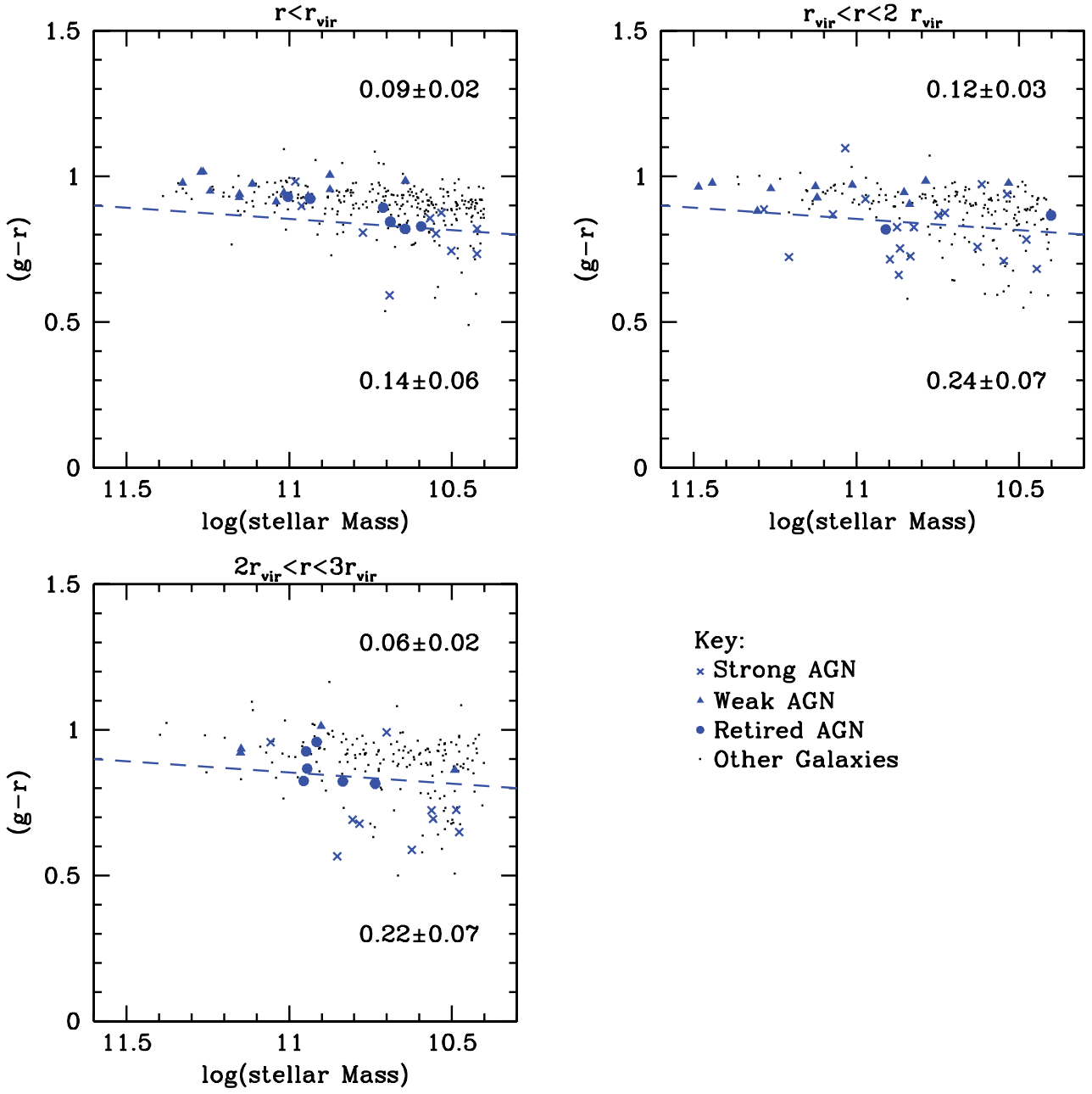

Figure 11. Colour–mass diagrams for our sample, split by radius to the cluster centre. AGN in our sample have been marked according to their WHAN classification from Fig. 8 (crosses for strong AGN; filled triangles for weak AGN; filled circles for the retired class). The dashed diagonal line is our approximation for the division between red sequence (above the line) and blue cloud galaxies (below the line). The numbers show the corresponding AGN fractions above and below this line. These fractions remain statistically constant with radius.

Table 7. AGN fractions derived from Fig. 11, divided by radius, colour and mass. The colour dividing line for blue cloud and red sequence is taken as the dashed line from Fig. 11, whereas the division in mass between massive and low-mass galaxies is at log(stellar mass) = 11.0.

Radius ($R_{\rm virial}$)	Massive red sequence	Low-mass red sequence	Massive blue cloud	Low-mass blue cloud
0–1	0.20 ± 0.06 (10/51)	0.06 ± 0.02 (13/207)	0.00 ± 0.00 (0/2)	0.15 ± 0.06 (6/40)
1–2	0.28 ± 0.09 (10/35)	0.08 ± 0.02 (10/128)	1.00 ± 1.00 (1/1)	0.22 ± 0.07 (11/50)
2–3	0.19 ± 0.11 (3/16)	0.05 ± 0.02 (6/120)	0.00 ± 0.00 (0/4)	0.23 ± 0.07 (11/47)

acknowledges support from the Australian Research Council via Discovery Project grant DP110102174.

Funding for the SDSS and SDSS-II has been provided by the Alfred P. Sloan Foundation, the Participating Institutions, the National Science Foundation, the US Department of Energy, the National Aeronautics and Space Administration, the Japanese Monbukagakusho, the Max Planck Society and the Higher Education Funding Council for England. The SDSS website is http://www.sdss.org/.

The SDSS is managed by the Astrophysical Research Consortium for the Participating Institutions. The Participating Institutions are the American Museum of Natural History, Astrophysical Institute Potsdam, the University of Basel, the University of Cambridge, Case Western Reserve University, the University of Chicago, Drexel University, Fermilab, the Institute for Advanced Study, the Japan Participation Group, Johns Hopkins University, the Joint Institute for Nuclear Astrophysics, the Kavli Institute for Particle Astrophysics and Cosmology, the Korean Scientist Group, the Chinese Academy of Sciences (LAMOST), Los Alamos National Laboratory, the Max-Planck-Institute for Astronomy (MPIA), the Max-Planck-Institute for Astrophysics (MPA), New Mexico State University, Ohio State University, the University of Pittsburgh, the University of Portsmouth, Princeton University, the United States Naval Observatory and the University of Washington.

This research has made use of the NASA/IPAC Extragalactic Database (NED) which is operated by the Jet Propulsion Laboratory, California Institute of Technology, under contract with the National Aeronautics andSpace Administration.

REFERENCES

Abazajian K. N. et al., 2009, ApJS, 182, 543
Abell G. O., Corwin H. G. Jr, Olowin R. P., 1989, ApJS, 70, 1
Andernach H., Tago E., Einasto M., Einasto J., Jaaniste J., 2005, in Fairall A. P., Woudt P. A., eds, ASP Conf. Ser. Vol. 329, Nearby Large-Scale Structures and the Zone of Avoidance. Astron. Soc. Pac., San Francisco, p. 283
Araya-Melo P. A., Reisenegger A., Meza A., van de Weygaert R., Dünner R., Quintana H., 2009, MNRAS, 399, 97
Atlee D. W., Martini P., Assef R. J., Kelson D. D., Mulchaey J. S., 2011, ApJ, 729, 22
Bahcall J. N., Kirhakos S., Saxe D. H., Schneider D. P., 1997, ApJ, 479, 642
Baldry I. K., Balogh M. L., Bower R. G., Glazebrook K., Nichol R. C., Bamford S. P., Budavari T., 2006, MNRAS, 373, 469
Baldwin J. A., Phillips M. M., Terlevich R., 1981, PASP, 93, 5
Best P. N., Kauffmann G., Heckman T. M., Brinchmann J., Charlot S., Ivezić Ž., White S. D. M., 2005, MNRAS, 362, 25
Brusa M. et al., 2009, A&A, 507, 1277
Burgett W. S. et al., 2004, MNRAS, 352, 605
Cameron E., 2011, PASA, 28, 128
Canalizo G., Stockton A., 2001, ApJ, 555, 719
Cid Fernandes R., Stasińska G., Schlickmann M. S., Mateus A., Vale Asari N., Schoenell W., Sodré L., 2010, MNRAS, 403, 1036
Cid Fernandes R., Stasińska G., Mateus A., Vale Asari N., 2011, MNRAS, 413, 1687
Coldwell G. V., Martínez H. J., Lambas D. G., 2002, MNRAS, 336, 207
Combes F., 2003, in Collin S., Combes F., Shlosman I., eds, ASP Conf. Ser. Vol. 290, Active Galactic Nuclei: From Central Engine to Host Galaxy. Astron. Soc. Pac., San Francisco, p. 411
Constantin A., Hoyle F., Vogeley M. S., 2008, ApJ, 673, 715
Dressler A., 1980, ApJ, 236, 351
Dressler A., Shectman S. A., 1988, AJ, 95, 985
Dressler A., Thompson I. B., Shectman S. A., 1985, ApJ, 288, 481
Dressler A. et al., 1997, ApJ, 490, 577
Dunlop J. S., McLure R. J., Kukula M. J., Baum S. A., O'Dea C. P., Hughes D. H., 2003, MNRAS, 340, 1095
Einasto M. et al., 2012, A&A, 540, A123
Fasano G., Franceschini A., 1987, MNRAS, 225, 155
Flin P., Krywult J., 2006, A&A, 450, 9
Floyd D. J. E., Kukula M. J., Dunlop J. S., Mclure R. J., Miller L., Percival W. J., Baum S. A., O'dea C. P., 2004, MNRAS, 355, 196
Floyd D. J. E., Dunlop J. S., Kukula M. J., Brown M. J. I., McLure R. J., Baum S. A., O'Dea C. P., 2012, MNRAS, in press (arXiv:1208.4143)
Gal R. R., de Carvalho R. R., Lopes P. A. A., Djorgovski S. G., Brunner R. J., Mahabal A., Odewahn S. C., 2003, AJ, 125, 2064
Gavazzi G., Savorgnan G., Fumagalli M., 2011, A&A, 534, A31
Georgakakis A., Gerke B. F., Nandra K., Laird E. S., Coil A. L., Cooper M. C., Newman J. A., 2008, MNRAS, 391, 183
Gilmour R., Gray M. E., Almaini O., Best P., Wolf C., Meisenheimer K., Papovich C., Bell E., 2007, MNRAS, 380, 1467
Girardi M., Giuricin G., Mardirossian F., Mezzetti M., Boschin W., 1998, ApJ, 505, 74
Gisler G. R., 1978, MNRAS, 183, 633
Haggard D., Green P. J., Anderson S. F., Constantin A., Aldcroft T. L., Kim D.-W., Barkhouse W. A., 2010, ApJ, 723, 1447
Haines C. P. et al., 2012, ApJ, 754, 97
Heckman T. M., Ptak A., Hornschemeier A., Kauffmann G., 2005, ApJ, 634, 161
Holden B. P. et al., 2007, ApJ, 670, 190
Hopkins P. F., Hernquist L., 2006, ApJS, 166, 1
Jahnke K. et al., 2004, ApJ, 614, 568
Jensen P. C., Pimbblet K. A., 2012, MNRAS, 422, 2841
Kauffmann G. et al., 2003, MNRAS, 346, 1055
Kauffmann G., White S. D. M., Heckman T. M., Ménard B., Brinchmann J., Charlot S., Tremonti C., Brinkmann J., 2004, MNRAS, 353, 713
Kaviraj S. et al., 2012, MNRAS, 423, 49
Kereš D., Katz N., Weinberg D. H., Davé R., 2005, MNRAS, 363, 2
Kewley L. J., Dopita M. A., Sutherland R. S., Heisler C. A., Trevena J., 2001, ApJ, 556, 121
Klesman A. J., Sarajedini V. L., 2012, MNRAS, 425, 1215
Koyama Y. et al., 2008, MNRAS, 391, 1758
Lee G.-H., Woo J.-H., Lee M. G., Hwang H. S., Lee J. C., Sohn J., Lee J. H., 2012, ApJ, 750, 141
Letawe Y., Letawe G., Magain P., 2010, MNRAS, 403, 2088
Lietzen H., Heinämäki P., Nurmi P., Liivamägi L. J., Saar E., Tago E., Takalo L. O., Einasto M., 2011, A&A, 535, A21
Lintott C. J. et al., 2008, MNRAS, 389, 1179
Lynden-Bell D., 1969, Nat, 223, 690
Mamon G. A., 1992, ApJ, 401, L3
Martini P., Mulchaey J. S., Kelson D. D., 2007, ApJ, 664, 761
Miller C. J., Nichol R. C., Gómez P. L., Hopkins A. M., Bernardi M., 2003, ApJ, 597, 142
Miller C. J. et al., 2005, AJ, 130, 968
Montero-Dorta A. D. et al., 2009, MNRAS, 392, 125
Moore B., Katz N., Lake G., Dressler A., Oemler A., 1996, Nat, 379, 613
Muldrew S. I. et al., 2012, MNRAS, 419, 2670
Nair P. B., Abraham R. G., 2010, ApJ, 714, L260
Owers M. S., Nulsen P. E. J., Couch W. J., 2011, ApJ, 741, 122
Pasquali A., van den Bosch F. C., Mo H. J., Yang X., Somerville R., 2009, MNRAS, 394, 38
Peacock J. A., 1983, MNRAS, 202, 615
Perez J., Tissera P., Padilla N., Alonso M. S., Lambas D. G., 2009, MNRAS, 399, 1157
Pimbblet K. A., 2011, MNRAS, 411, 2637
Pimbblet K. A., Jensen P. C., 2012, MNRAS, 426, 1632
Pimbblet K. A., Smail I., Kodama T., Couch W. J., Edge A. C., Zabludoff A. I., O'Hely E., 2002, MNRAS, 331, 333
Pimbblet K. A., Smail I., Edge A. C., O'Hely E., Couch W. J., Zabludoff A. I., 2006, MNRAS, 366, 645
Pinkney J., Roettiger K., Burns J. O., Bird C. M., 1996, ApJS, 104, 1
Plionis M., Tovmassian H. M., Andernach H., 2009, MNRAS, 395, 2

Popesso P., Biviano A., 2006, A&A, 460, L23
Porter S. C., Raychaudhury S., Pimbblet K. A., Drinkwater M. J., 2008, MNRAS, 388, 1152
Reichard T. A. et al., 2009, ApJ, 691, 1005
Richstone D. et al., 1998, Nat, 395, A14
Ruderman J. T., Ebeling H., 2005, ApJ, 623, L81
Sanders D. B., Soifer B. T., Elias J. H., Madore B. F., Matthews K., Neugebauer G., Scoville N. Z., 1988, ApJ, 325, 74
Schawinski K., Thomas D., Sarzi M., Maraston C., Kaviraj S., Joo S.-J., Yi S. K., Silk J., 2007, MNRAS, 382, 1415
Shabala S. S. et al., 2012, MNRAS, 423, 59
Sheth K. et al., 2008, ApJ, 675, 1141
Sivakoff G. R., Martini P., Zabludoff A. I., Kelson D. D., Mulchaey J. S., 2008, ApJ, 682, 803
Smirnova A. A., Moiseev A. V., Afanasiev V. L., 2010, MNRAS, 408, 400
Smith G. P., Treu T., Ellis R. S., Moran S. M., Dressler A., 2005, ApJ, 620, 78
Spergel D. N. et al., 2007, ApJS, 170, 377
Strauss M. A. et al., 2002, AJ, 124, 1810
Struble M. F., Ftaclas C., 1994, AJ, 108, 1
Tanaka M., 2012, PASJ, 64, 37
Tremonti C. A. et al., 2004, ApJ, 613, 898
Urrutia T., Lacy M., Becker R. H., 2008, ApJ, 674, 80
Veilleux S., Osterbrock D. E., 1987, ApJS, 63, 295
von der Linden A., Wild V., Kauffmann G., White S. D. M., Weinmann S., 2010, MNRAS, 404, 1231
Xue Y. Q. et al., 2010, ApJ, 720, 368
Yan R., Blanton M. R., 2012, ApJ, 747, 61
Yun M. S., Reddy N. A., Condon J. J., 2001, ApJ, 554, 803

APPENDIX A: ABELL 1620

Abell 1620 is noted in Section 2 as possessing significant substructure at $>2R_{\rm virial}$, in agreement with Burgett et al. (2004).

In Fig. A1 we plot a smoothed surface density of galaxy members for this cluster. This figure reveals two overdensities of galaxies to the south-east of Abell 1620 proper. We identify these two overdensities as SDSS-C4 1010 (Miller et al. 2005) at $12^{\rm h}\,48^{\rm m}\,02\overset{\rm s}{.}7\ -01^{\rm d}\,39^{\rm m}\,10^{\rm s}$, and NSC J124857−015532 (Gal et al. 2003) at $12^{\rm h}\,48^{\rm m}\,57\overset{\rm s}{.}7\ -01^{\rm d}\,55^{\rm m}\,33^{\rm s}$ using NED.

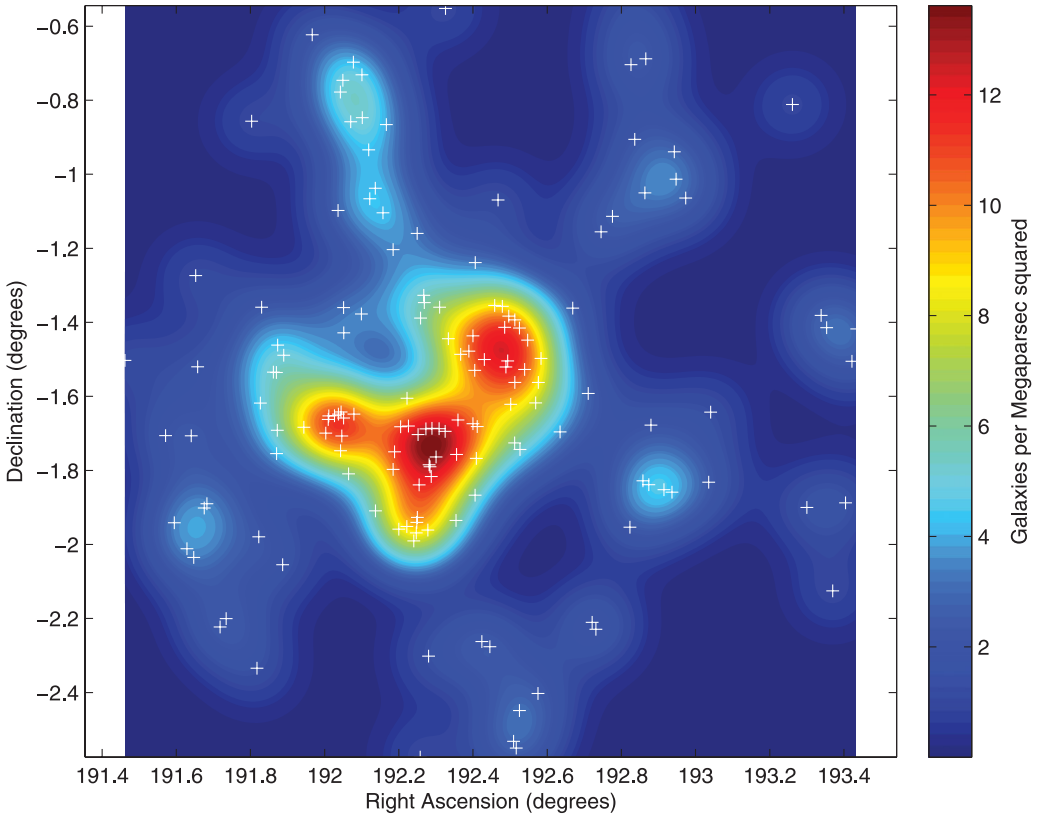

Figure A1. Space density of our bias-corrected galaxy sample for Abell 1620. The galaxies (white crosses) have been smoothed with an (arbitrary) Gaussian kernel of $0\overset{\circ}{.}1$ in length and the density represented by the variation in colour (see the side colour bar). The centre of the plot corresponds to the position of the brightest cluster galaxy in Abell 1620 and is also the luminosity-weighted centre. Two other peaks in the spatial distribution are seen at $12^{\rm h}\,48^{\rm m}\,02\overset{\rm s}{.}7\ -01^{\rm d}\,39^{\rm m}\,10^{\rm s}$ and $12^{\rm h}\,48^{\rm m}\,57\overset{\rm s}{.}7\ -01^{\rm d}\,55^{\rm m}\,33^{\rm s}$ that we identify as SDSS-C4 1010 and NSC J124857−015532, respectively. Although these secondary peaks appear significant in space density, their masses are less than the primary A1620 cluster, in agreement with Burgett et al. (2004).

These subclusters (i.e. groups) are notable in our analysis. In Fig. 9, there is a local peak in Σ_5 at 1.2–1.5$R_{\rm virial}$. We associate this peak with these two groups. Of note, there are two AGN contained in this peak (i.e. with $\log(\Sigma_5) > 1.8$). It is these AGN that result in the enhanced Σ_5 average value noted in Table 5 at these radii. We explicitly note that the masses of these secondary peaks are less than the primary A1620 peak (as confirmed by Burgett et al. 2004). We further emphasize that removal of Abell 1620 from our analysis does not change the primary results contained in our work. Therefore, we regard these two overdensities to have had negligible effect on the AGN contained within it (i.e. no enhancement), in line with our conclusions.

This paper has been typeset from a TEX/LATEX file prepared by the author.